

# Quasi-elastic neutrino charged-current scattering off $^{12}\text{C}$

A. V. Butkevich

*Institute for Nuclear Research, Russian Academy of Sciences,  
60th October Anniversary Prosp. 7A, Moscow 117312, Russia*

(Dated: November 12, 2018)

The charged-current quasi-elastic scattering of muon neutrino on a carbon target is calculated for neutrino energy up to 2.8 GeV using the relativistic distorted-wave impulse approximation with relativistic optical potential, which was earlier successfully applied to describe electron-nucleus data. We studied both neutrino and electron processes and have shown that the reduced exclusive cross section for neutrino and electron scattering are similar. We have also studied nuclear and axial vector mass effects on the shape of  $Q^2$  distribution. The comparison of the (anti)neutrino total cross sections per (proton)neutron, calculated for the carbon and oxygen targets shows the cross sections for oxygen to be lower than those for carbon. We found significant nuclear model dependence of inclusive and total cross sections for energy about 1 GeV.

PACS numbers: 25.30.-c, 25.30.Bf, 25.30.Pt, 13.15.+g

## I. INTRODUCTION

The goals of the current and planned set of accelerator-based neutrino experiments [1–7] are the precision measurements of the neutrino mass squared difference  $\Delta m_{23}^2$  by measuring muon neutrino disappearance, and searching for the last unmeasured leptonic mixing angle  $\theta_{13}$  through the muon to electron neutrino transition. The last oscillation channel, if it occurs, opens the possibility of observation matter/anti-matter asymmetries in neutrinos and determination of the ordering of the neutrino mass states. The data of these experiments will greatly extend the statistics due to extremely intense neutrino beamline.

To study the neutrino oscillation effects on the terrestrial distance scale, the neutrino beams cover the energy range from a few hundred MeV to several GeV. In this energy range, the dominant contribution to the neutrino-nucleus cross section comes from the charged-

current (CC) quasi-elastic (QE) reactions and resonance production processes. The cross section data in this energy range are rather scarce and were taken on the targets, which are not used in the neutrino oscillation experiments (i.e. water, iron, lead or plastic). In this situation, the statistical uncertainties should be negligible as compared to systematic errors in the incident neutrino flux, neutrino interaction model and the detector effects on the neutrino events selection and neutrino energy reconstruction. Apparently, these uncertainties produce systematic errors in the extraction of oscillation parameters.

Many experiments try to reduce these uncertainties by using a near detectors. One of the options for near detector design is to make the near detector as more segmented and fine-grained, using scintillator (carbon) as a target and detecting material. This strategy means that one must try to measure the fluxes and cross sections as independently as possible, and then use this information to constrain the detector simulation so that the information is correctly extrapolated to the far detector. The concern with this strategy is that the detector simulation must accurately predict the detector response. Because the near and far detectors are not necessarily of the same target material, a part of the near detector must include some of the same target material, so that nuclear effects on the cross sections (QE and non-QE) could be taken into account. Among the proposed experiments MINERvA [4] and ND280 detector [8] will have the possibility for precise measurements in a wide range of energies and for various nuclear targets.

To model the QE neutrino scattering from a nucleus, the most part of the Monte Carlo (MC) event generators [9] are based on the relativistic Fermi gas model (RFGM) [10] with Pauli blocking, in which the nucleus is described as a system of quasi-free nucleons with a flat nucleon momentum distribution up to the same Fermi momentum  $p_F$  and nuclear binding energy  $\epsilon_b$ . But this model does not take into account the nuclear shell structure, the final state interaction (FSI) between the outgoing nucleon and residual nucleus and the presence of short-range nucleon-nucleon ( $NN$ ) correlations, leading to appearance of a high-momentum and high-energy component in the nucleon momentum-energy distribution in the target.

The comparison with the high-precision electron scattering data has shown [11] that the accuracy of the RFGM prediction becomes poor at low squared four-momentum transfer  $Q^2$ , where the nuclear effects are largest. The modern quasi-elastic neutrino scattering data (the CC QE event distribution as a function of  $Q^2$ ) [1, 12] also reveal the inadequacies in

the present neutrino cross section simulation. The data/MC disagreement shows the data deficit in the low- $Q^2$  ( $Q^2 \leq 0.2$  (GeV/c) $^2$ ) region.

There are many calculations for the QE neutrino charged-current and neutral-current scattering cross sections on nucleus, which go beyond the simple RFGM and use more realistic description of nuclear dynamics. In calculation of Refs.[13, 14] within the plane-wave impulse approximation (PWIA), the short range  $NN$ -correlations were included using the description of nuclear dynamics, based on nuclear many body theory. Charged current and/or neutral current neutrino-nucleus cross sections were studied within the relativistic distorted-wave impulse approximation (RDWIA) in Refs.[15–24], using the relativistic shell model approach and taking into account the FSI effects. In Refs.[21, 22] the contribution of the short range correlations (SRC) was also considered. The FSI effects were studied in Refs.[25–28] within the framework of the random phase approximation, in Refs.[29–31] - within a Superscaling approach, and in Ref.[32] - in a GiBUU model.

In this paper, we calculate the single-nucleon knockout contribution to the exclusive, inclusive and total cross sections of charged-current QE (anti)neutrino scattering from  $^{12}\text{C}$ , using different approximations (PWIA and RDWIA) and the Fermi gas model. We employ the LEA code [33] which was adopted for neutrino reactions. In our approach, the effect of the SCR in the carbon ground state is evaluated in the PWIA [34, 35] and the FSI effect on the inclusive cross sections in the presence of the  $NN$ -correlations is estimated according Ref.[21]. The aims of this work are a) calculation the RDWIA CC QE  $\nu^{12}\text{C}$  cross sections, b) investigation of nuclear effects on the  $Q^2$  dependence of the (anti)neutrino cross section, and c) comparison of the total cross sections, scaled with the number of neutron/proton in the target for (anti)neutrino scattering on the oxygen and carbon targets.

The outline of this paper is the following. In Sec. II we present briefly the formalism for the CC QE scattering process and the RDWIA model. The results are presented and discussed in Sec. III. Our conclusions are summarized in Sec. IV.

## II. FORMALISM OF QUASI-ELASTIC SCATTERING AND RDWIA

We consider electron and neutrino charged-current QE exclusive

$$l(k_i) + A(p_A) \rightarrow l'(k_f) + N(p_x) + B(p_B), \quad (1)$$

and inclusive

$$l(k_i) + A(p_A) \rightarrow l'(k_f) + X \quad (2)$$

scattering off nuclei in one-photon (W-boson) exchange approximation. Here  $l$  labels the incident lepton [electron or muon (anti)neutrino], and  $l'$  represents the scattered lepton (electron or muon),  $k_i = (\varepsilon_i, \mathbf{k}_i)$  and  $k_f = (\varepsilon_f, \mathbf{k}_f)$  are the initial and final lepton momenta,  $p_A = (\varepsilon_A, \mathbf{p}_A)$ , and  $p_B = (\varepsilon_B, \mathbf{p}_B)$  are the initial and final target momenta,  $p_x = (\varepsilon_x, \mathbf{p}_x)$  is the ejectile nucleon momentum,  $q = (\omega, \mathbf{q})$  is the momentum transfer carried by the virtual photon (W-boson), and  $Q^2 = -q^2 = \mathbf{q}^2 - \omega^2$  is the photon (W-boson) virtuality.

### A. CC QE neutrino-nucleus cross sections

In the laboratory frame, the differential cross section for the exclusive electron ( $\sigma^{el}$ ) and (anti)neutrino CCQE ( $\sigma^{cc}$ ) scattering, in which only a single discrete state or narrow resonance of the target is excited, can be written as

$$\frac{d^5\sigma^{el}}{d\varepsilon_f d\Omega_f d\Omega_x} = R \frac{|\mathbf{p}_x| \varepsilon_x \varepsilon_f \alpha^2}{(2\pi)^3 \varepsilon_i Q^4} L_{\mu\nu}^{(el)} W^{\mu\nu(el)} \quad (3a)$$

$$\frac{d^5\sigma^{cc}}{d\varepsilon_f d\Omega_f d\Omega_x} = R \frac{|\mathbf{p}_x| \varepsilon_x |\mathbf{k}_f| G^2 \cos^2 \theta_c}{(2\pi)^5 \varepsilon_i 2} L_{\mu\nu}^{(cc)} W^{\mu\nu(cc)}, \quad (3b)$$

where  $\Omega_f$  is the solid angle for the lepton momentum,  $\Omega_x$  is the solid angle for the ejectile nucleon momentum,  $\alpha \simeq 1/137$  is the fine-structure constant,  $G \simeq 1.16639 \times 10^{-11}$  MeV<sup>-2</sup> is the Fermi constant,  $\theta_C$  is the Cabbibo angle ( $\cos \theta_C \approx 0.9749$ ),  $L_{\mu\nu}$  is the lepton tensor and  $W_{\mu\nu}^{(el)}$  and  $W_{\mu\nu}^{(cc)}$  are, respectively, the electromagnetic and weak CC nuclear tensors. The recoil factor  $R$  is given by

$$R = \int d\varepsilon_x \delta(\varepsilon_x + \varepsilon_B - \omega - m_A) = \left| 1 - \frac{\varepsilon_x \mathbf{p}_x \cdot \mathbf{p}_B}{\varepsilon_B \mathbf{p}_x \cdot \mathbf{p}_x} \right|^{-1}, \quad (4)$$

and  $\varepsilon_x$  is the solution to the equation

$$\varepsilon_x + \varepsilon_B - m_A - \omega = 0, \quad (5)$$

where  $\varepsilon_B = \sqrt{m_B^2 + \mathbf{p}_B^2}$ ,  $\mathbf{p}_B = \mathbf{q} - \mathbf{p}_x$ ,  $\mathbf{p}_x = \sqrt{\varepsilon_x^2 - m^2}$ , and  $m_A$ ,  $m_B$ , and  $m$  are masses of the target, recoil nucleus and nucleon, respectively. The missing momentum  $p_m$  and missing energy  $\varepsilon_m$  are defined by

$$\mathbf{p}_m = \mathbf{p}_x - \mathbf{q} \quad (6a)$$

$$\varepsilon_m = m + m_B - m_A \quad (6b)$$

The leptonic tensor is separated into a symmetrical and an anti-symmetrical components that are written as in Ref. [21]. The electromagnetic and weak CC hadronic tensors,  $W_{\mu\nu}^{(el)}$  and  $W_{\mu\nu}^{(cc)}$  are given by bilinear products of the transition matrix elements of the nuclear electromagnetic or CC operator  $J_\mu^{(el)(cc)}$  between the initial nucleus state  $|A\rangle$  and the final state  $|B_f\rangle$  as

$$W_{\mu\nu}^{(el)(cc)} = \sum_f \langle B_f, p_x | J_\mu^{(el)(cc)} | A \rangle \langle A | J_\nu^{(el)(cc)\dagger} | B_f, p_x \rangle, \quad (7)$$

where the sum is taken over undetected states.

In the inclusive reactions (2) only the outgoing lepton is detected, and the differential cross sections can be written as

$$\frac{d^3\sigma^{el}}{d\varepsilon_f d\Omega_f} = \frac{\varepsilon_f \alpha^2}{\varepsilon_i Q^4} L_{\mu\nu}^{(el)} \mathcal{W}^{\mu\nu(el)}, \quad (8a)$$

$$\frac{d^3\sigma^{cc}}{d\varepsilon_f d\Omega_f} = \frac{1}{(2\pi)^2} \frac{|\mathbf{k}_f| G^2 \cos^2 \theta_c}{\varepsilon_i} L_{\mu\nu}^{(cc)} \mathcal{W}^{\mu\nu(cc)}, \quad (8b)$$

where  $\mathcal{W}^{\mu\nu}$  is the inclusive hadronic tensor. The expressions for the exclusive (3) and inclusive (8) lepton scattering cross sections in terms of response functions are given in Ref.[21].

It is also useful to define a reduced cross section

$$\sigma_{red} = \frac{d^5\sigma}{d\varepsilon_f d\Omega_f d\Omega_x} / K^{(el)(cc)} \sigma_{lN}, \quad (9)$$

where are phase-space factors for electron and neutrino scattering, the recoil factor  $R$  is given by Eq.(4), and  $\sigma_{lN}$  is the corresponding elementary cross section for the lepton scattering from the moving free nucleon.

## B. Models

We describe the lepton-nucleon scattering in the impulse approximation (IA), in which only one nucleon of the target is involved in the reaction, and the nuclear current is written as a sum of single-nucleon currents. Then, the nuclear matrix element in Eq.(7) takes the form

$$\langle p, B | J^\mu | A \rangle = \int d^3r \exp(i\mathbf{t} \cdot \mathbf{r}) \bar{\Psi}^{(-)}(\mathbf{p}, \mathbf{r}) \Gamma^\mu \Phi(\mathbf{r}), \quad (10)$$

where  $\Gamma^\mu$  is the vertex function,  $\mathbf{t} = \varepsilon_B \mathbf{q}/W$  is the recoil-corrected momentum transfer,  $W = \sqrt{(m_A + \omega)^2 - \mathbf{q}^2}$  is the invariant mass,  $\Phi$  and  $\Psi^{(-)}$  are relativistic bound-state and outgoing wave functions.

For electron scattering, we use the CC2 electromagnetic vertex function for a free nucleon [36]

$$\Gamma^\mu = F_V^{(el)}(Q^2)\gamma^\mu + i\sigma^{\mu\nu}\frac{q_\nu}{2m}F_M^{(el)}(Q^2), \quad (11)$$

where  $\sigma^{\mu\nu} = i[\gamma^\mu, \gamma^\nu]/2$ ,  $F_V^{(el)}$  and  $F_M^{(el)}$  are the Dirac and Pauli nucleon form factors. The single-nucleon charged current has  $V-A$  structure  $J^{\mu(cc)} = J_V^\mu + J_A^\mu$ . For the free-nucleon vertex function  $\Gamma^{\mu(cc)} = \Gamma_V^\mu + \Gamma_A^\mu$  we use the CC2 vector current vertex function

$$\Gamma_V^\mu = F_V(Q^2)\gamma^\mu + i\sigma^{\mu\nu}\frac{q_\nu}{2m}F_M(Q^2) \quad (12)$$

and the axial current vertex function

$$\Gamma_A^\mu = F_A(Q^2)\gamma^\mu\gamma_5 + F_P(Q^2)q^\mu\gamma_5. \quad (13)$$

The weak vector form factors  $F_V$  and  $F_M$  can be expressed in terms of the corresponding electromagnetic factors for proton  $F_{i,p}^{(el)}$  and neutron  $F_{i,n}^{(el)}$  as follows

$$F_i = F_{i,p}^{(el)} - F_{i,n}^{(el)}. \quad (14)$$

For the electromagnetic and weak CC vector vertexes we employ the de Forest prescription [36] (because the bound nucleons are off shell) and Coulomb gauge. For the Dirac and Pauli nucleon form factors we use the approximation from Ref. [37] and the dipole approximation for the axial  $F_A$  and pseudoscalar  $F_P$  form factors

$$F_A(Q^2) = \frac{F_A(0)}{(1 + Q^2/M_A^2)^2}, \quad F_P(Q^2) = \frac{2mF_A(Q^2)}{m_\pi^2 + Q^2}, \quad (15)$$

where  $F_A(0) = 1.267$  and  $m_\pi$ ,  $M_A$  are the pion and axial mass, respectively.

In Ref. [38], a formalism was developed for the  $A(e, e'N)B$  reaction that describes channel coupling in the FSI of the  $N + B$  system. In this work the independent particle shell model (IPSM) is assumed for nuclear structure. The model space for  $^{12}\text{C}(l, l'N)$  consists of  $1s_{1/2}$  and  $1p_{3/2}$  nucleon-hole states in the  $^{11}\text{B}$  and  $^{11}\text{C}$  nuclei. The  $1s_{1/2}$  state is regarded as a discrete state even though its spreading width is actually appreciable.

In the independent particle shell model the relativistic bound-state functions  $\Phi$  in Eq.(10) are obtained within the Hartree–Bogoliubov approximation in the  $\sigma - \omega$  model [39]. The

upper component of the bound-state wave function  $\Phi$  is used for calculation of the shell nucleons spectral function in the PWIA calculations. We use the nucleon bound-state functions calculated by the TIMORA code [40] with the normalization factors  $S(\alpha)$  relative to full occupancy of the IPSM orbitals of  $^{12}\text{C}$ :  $S(1p_{3/2})=84\%$ ,  $S(1s_{1/2})=100\%$ , and an average factor of about 89%. These estimations of the depletion of hole states follow from the RDWIA analysis of  $^{12}\text{C}(e, e'p)$  for  $Q^2 < 2$  (GeV/c) $^2$  [41] and consist with a direct measurement of the spectral function using  $^{12}\text{C}(e, e'p)$  in parallel kinematics [42], which observed approximately 0.6 protons in a region with  $p_m \geq 240$  Mev/c and  $\varepsilon_m \geq 50$  MeV attributable to a single-nucleon knockout from correlated cluster. Similar estimates of the depletion of hole states are available from the self-consistent Green's function method [43], correlated basis function theory [44] and other method also.

In the RDWIA the ejectile wave function  $\Psi$  in Eq.(10) is obtained following the direct Pauli reduction method [45, 46]. It is well known that the Dirac spinor

$$\Psi = \begin{pmatrix} \Psi_+ \\ \Psi_- \end{pmatrix} \quad (16)$$

can be written in terms of its positive energy component  $\Psi_+$  as

$$\Psi = \begin{pmatrix} \Psi_+ \\ \frac{\boldsymbol{\sigma} \cdot \mathbf{p}}{E+M+S-V} \Psi_+ \end{pmatrix}, \quad (17)$$

where  $S = S(r)$  and  $V = V(r)$  are the scalar and vector potentials for the nucleon with energy  $E$ . The upper component  $\Psi_+$  can be related to the Schrödinger-like wave function  $\xi$  by the Darwin factor  $D(r)$ , i.e.

$$\Psi_+ = \sqrt{D(r)} \xi, \quad (18)$$

$$D(r) = \frac{E + M + S(r) - V(r)}{E + M}. \quad (19)$$

The two-component wave function  $\xi$  is the solution of the Schrödinger equation containing equivalent central and spin-orbit potentials, which are functions of the scalar and vector potentials  $S$  and  $V$ , and are energy dependent. We use the LEA program [33] for numerical calculation of the distorted wave functions with EDAD1 SV relativistic optical potential [47] for carbon.

In the Plane-Wave Impulse Approximation (PWIA) the final state interaction between the outgoing nucleon and the residual nucleus is neglected, and the nonrelativistic PWIA exclusive cross section has a factorized form [48]

$$\frac{d^5\sigma}{d\varepsilon_f d\Omega_f d\Omega_x} = K^{(el)(cc)} \sigma_{iN} \mathcal{P}(E, \mathbf{p}) \quad (20)$$

where  $\mathcal{P}(E, \mathbf{p})$  is the nuclear spectral function.

According to the JLab data [42, 49], the occupancy of the independent particle shell model orbitals of  $^{12}\text{C}$  equals about 89%, on the average. In this work we assume that the missing strength (11%) can be attributed to the short-range  $NN$ -correlations in the ground state, leading to appearance of high-momentum (HM) and high-energy nucleon distribution in the target. In order to estimate this effect in the inclusive cross sections, we consider the phenomenological model [34, 35] where the high-momentum (HM) part of the spectral function is determined by excited states with one or more nuclei in a continuum.

We calculate the inclusive cross sections with the FSI effects in the presence of the short-range  $NN$ -correlations, using the approach which was proposed in Ref.[21].

### III. RESULTS AND ANALYSIS

#### A. Electron scattering

The LEA code was successfully tested against  $^{12}\text{C}(e, e'p)$  data. For illustration, Fig.1 shows measured JLab [49] reduced cross sections for the removal of protons from the 1s and 1p shells of  $^{12}\text{C}$  as functions of missing momentum  $p_m$  as compared with LEA code calculations. It should be noted that negative values of  $p_m$  correspond to  $\phi = \pi$  and positive ones to  $\phi=0$ , where  $\phi$  is the angle between the scattering  $(\mathbf{k}_i, \mathbf{k}_f)$  and reaction  $(\mathbf{p}_x, \mathbf{p}_B)$  planes. The data for beam energy  $E_{beam}=2.445$  GeV and  $Q^2=0.6, 1.2,$  and  $1.8$  (GeV/c) $^2$  were measured in the quasi-perpendicular kinematics with constant  $(\omega, \mathbf{q})$ . The detailed analysis data [41] for  $^{12}\text{C}(e, e'p)$  with  $Q^2 \leq 2$  (GeV/c) $^2$  using the RDWIA based upon Dirac-Hartree wave functions has shown that the 1p normalization extracted from data for  $Q^2 \geq 0.6$  (GeV/c) $^2$  is equals approximately 0.87, independent of  $Q^2$ . The total 1p and 1s strength for  $\varepsilon_m \leq 80$  MeV approaches 100% of IPSM, consistent with a continuum contribution for  $30 \leq \varepsilon_m \leq 80$  MeV of about 12% of IPSM.



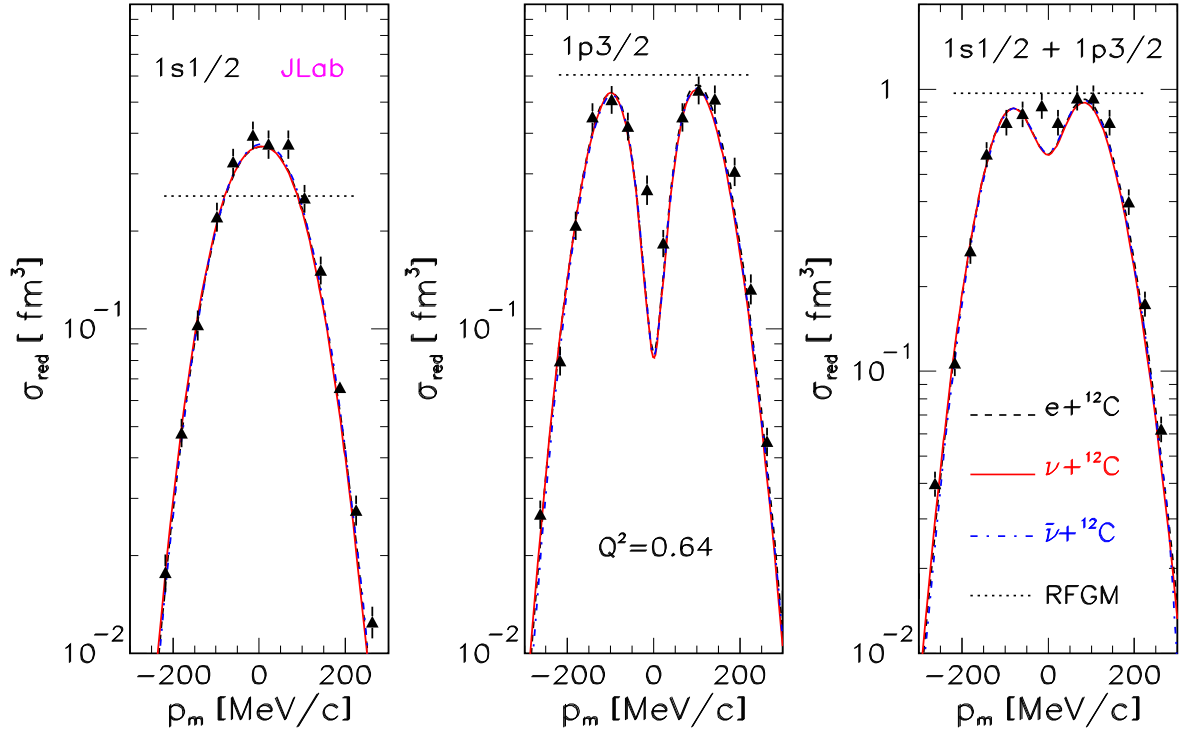


FIG. 1: (Color online) Comparison of the RDWIA and the RFGM calculations for electron, neutrino and antineutrino reduced cross sections for the removal of nucleons from 1p and 1s shells of  $^{12}\text{C}$  as functions of missing momentum. JLab data [49] for beam energy  $E_{beam}=2.455$  GeV, proton kinetic energy  $T_p=350$  MeV, and  $Q^2=0.64$   $(\text{GeV}/c)^2$ . The RDWIA calculations are shown for electron scattering (dashed line) and neutrino (solid line) and antineutrino (dashed-dotted line) scattering; and the RFGM results are shown for the reduced cross sections (dotted line) for the JLab kinematics.

The electron and neutrino scattering off the nuclei are closely interrelated and one can treat both processes within the same formalism. In the nonrelativistic PWIA,  $\sigma_{red}$  is a nuclear spectral function and should be similar for electron and (anti)neutrino scattering except small distinctions which can be attributed to the Coulomb distortion upon the electron wave function. The small difference between neutrino and antineutrino is due to difference in the FSI of the proton and neutron with the residual nucleus. This effect is neglected at the energy beam higher than 1 GeV. There is an overall good agreement between calculated in the RDWIA electron and (anti)neutrino cross sections and data. Apparently the RFGM predictions (with the Fermi momentum  $p_F=221$  MeV/c and binding energy  $\epsilon_b=25$  MeV)

overestimate the values of cross sections and completely off the exclusive data. This is due to the uniform momentum distribution of the Fermi gas model and neglecting by the FSI effects. Therefore, the RFGM can not predict well enough the momentum distribution of outgoing protons in simulation of the CC QE two-track events at momentum transfer  $|\mathbf{q}| \leq |\mathbf{p}_m|$ , i.e. at low  $Q^2$ .

A complex relativistic optical potential with a nonzero imaginary part generally produces an absorption of flux. However, for the inclusive reaction, the total flux must conserve. Currently there is no fully consistent solution to this problem, and different approaches are used. In Refs.[15, 50] it was shown that the inclusive CC cross sections calculated with only the real part of the optical potential are almost identical those of the Green's function approach, in which the FSI effect in the inclusive reactions is treated by means of a complex optical potential and the total flux is conserved. In this work, in order to calculate the inclusive and total cross sections, we use the approach, in which only the real part of the optical potential EDAD1 is included.

To test our approach, we calculated the inclusive  $^{12}\text{C}(e, e')$  cross sections and compared them with data from SLAC [51–53], from Saclay [54], and from JLab [55]. Figures 2 and 3 show measured inclusive cross sections as functions of energy transfer as compared to the RDWIA, PWIA, and RFGM calculations. These data cover the range of the tree-momentum transfer (around the peak) from  $|\mathbf{q}| \approx 310$  MeV/c (beam energy  $E_e=1500$  MeV and scattering angle  $\theta=11.95^\circ$ ) up to  $|\mathbf{q}| \approx 530$  MeV/c ( $E_e=2020$  MeV,  $\theta=15^\circ$ ). We note that, relative to the PWIA results, the generic effect of the FSI with the real part of the optical potential is to reduce the cross section value around the peak and to shift the peak toward the lower value energy transfer. The inclusion of the high-momentum component increases the inclusive cross section in the high-energy transfer region and improves the agreement with data. For the RDWIA results, the difference between the calculated and measured cross sections at the maximum is less than  $\pm 12\%$ . For the RFGM results these difference decreases with  $|\mathbf{q}|$  from about 20% at  $|\mathbf{q}| \approx 310$  MeV/c down to  $\approx 13\%$  at  $|\mathbf{q}| \approx 510$  MeV/c. These results demonstrate a strong nuclear-model dependence of the inclusive cross sections at low momentum transfer.

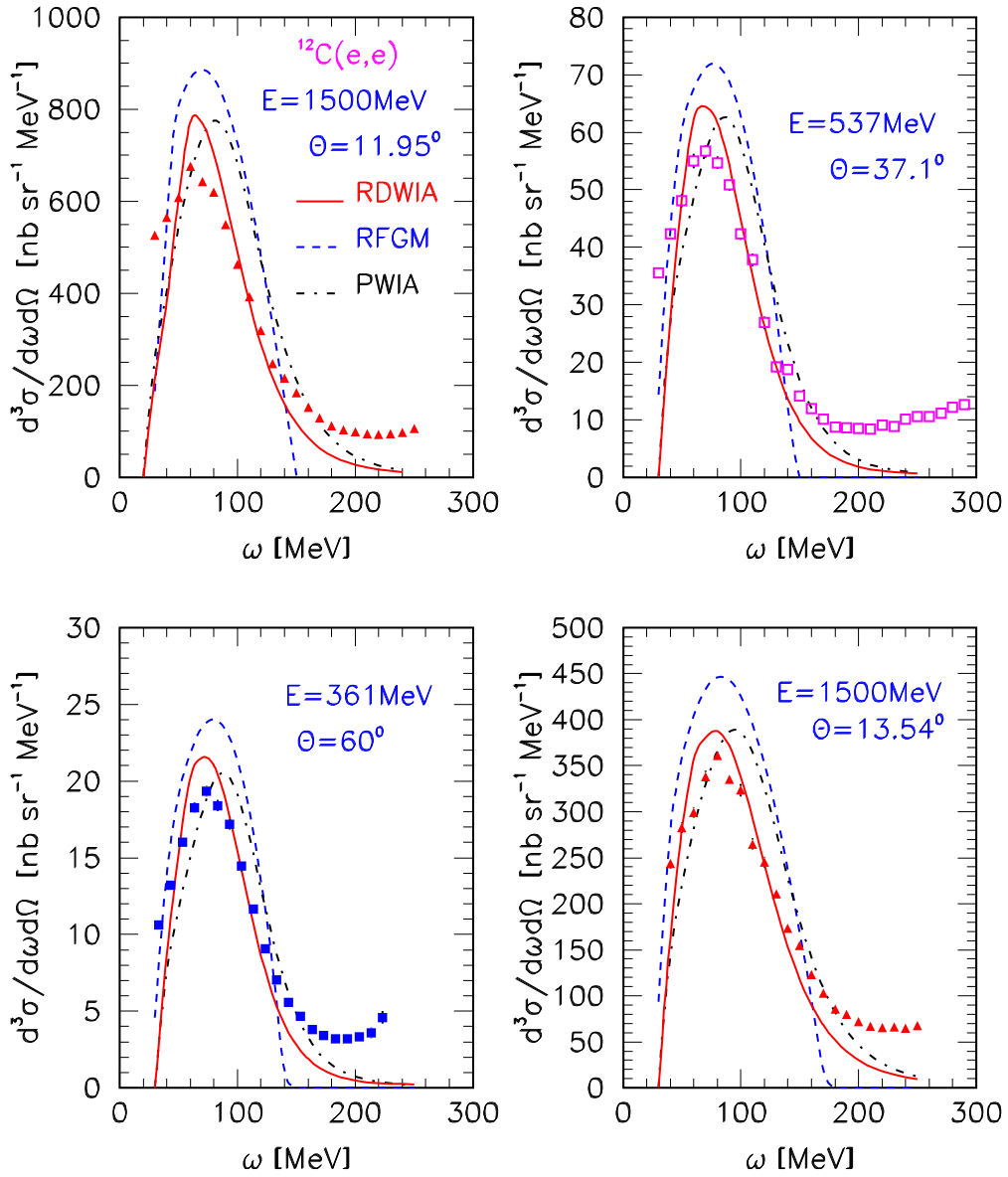


FIG. 2: (Color online) Inclusive cross section versus energy transfer  $\omega$  for electron scattering on  $^{12}\text{C}$ . The data are from Ref.[51] (filled triangles), Ref.[52] (open squares), and Ref.[54] (filled squares). In Ref.[51] data are for the electron beam energy  $E_e=1500$  MeV, and scattering angles  $\theta_e=11.95^\circ$ ,  $13.54^\circ$ ; in Ref.[52] data are for  $E_e=537$  MeV and  $\theta_e=37.1^\circ$ ; in Ref.[54] data are for  $E_e=361$  MeV and  $\theta_e=60^\circ$ .

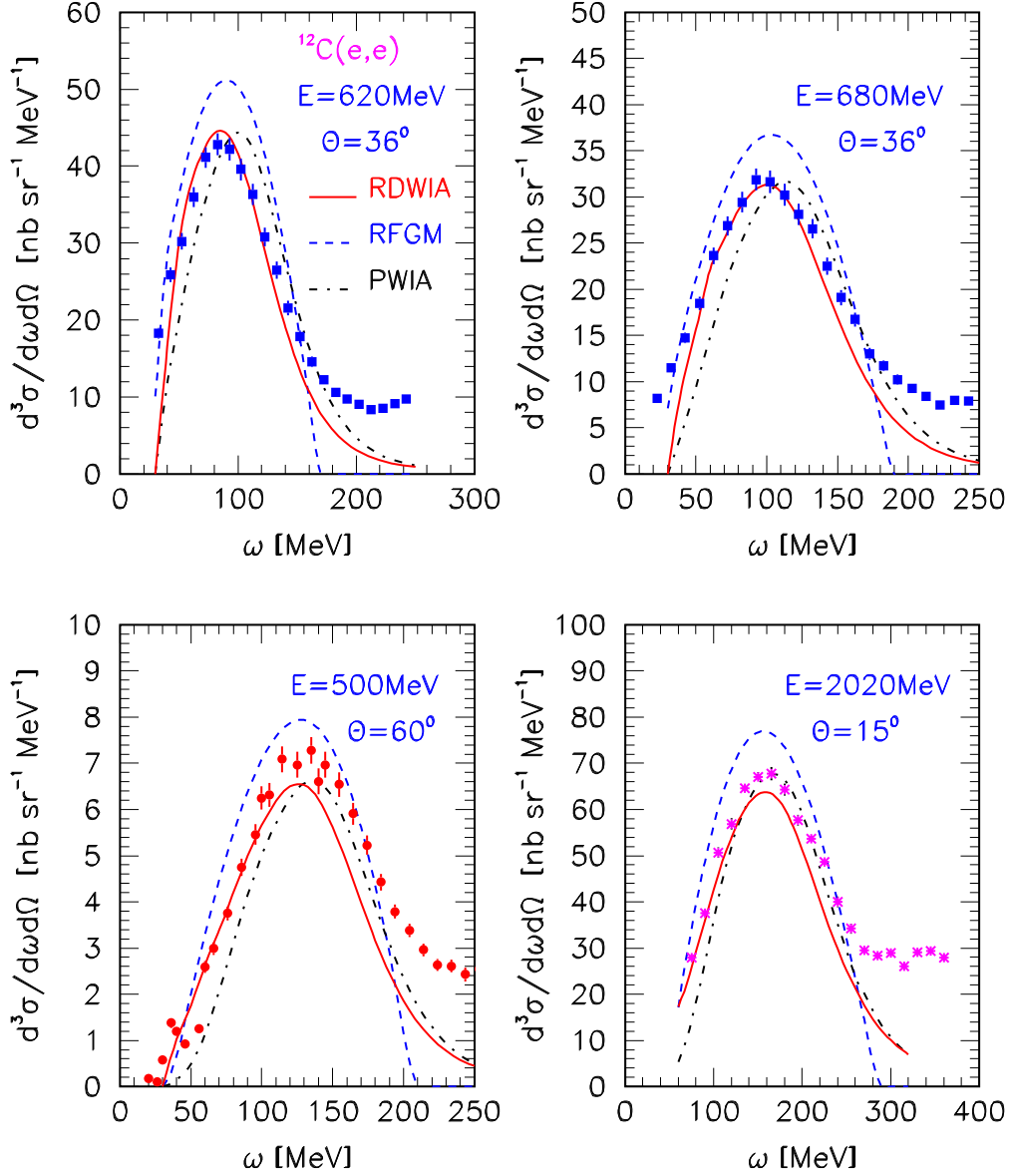


FIG. 3: (Color online) Same as Fig.2, but the data are from Ref.[54] (filled squares) for  $E_e=620$  MeV,  $\theta_e=36^\circ$  and  $E_e=680$  MeV,  $\theta_e=36^\circ$ ; Ref.[53] (filled circles) for  $E_e=500$  MeV,  $\theta_e=60^\circ$ ; Ref.[55] (stars) for  $E_e=2020$  MeV,  $\theta_e=15^\circ$ .

### B. Neutrino scattering

The charged-current QE events distributions as functions of  $Q^2$  were measured in K2K [12, 56] and MiniBooNE [1] experiments. The shape of the  $Q^2$  distribution, which is weakly dependent on the flux uncertainties, was analyzed. High statistic data show a disagreement

with the RFGM predictions. The data samples exhibit significant deficit in the region of low  $Q^2 \leq 0.2$  (GeV/c)<sup>2</sup> (so call low- $Q^2$  problem). In Ref.[1] it was shown that the data/MC disagreement is not due to mis-modeling of the incoming neutrino energy spectrum, but to inaccuracy in the simulation of CC QE interactions. To tune the Fermi gas model to the low  $Q^2$ , an additional parameter  $\kappa$  was introduced which reduced the phase space volume of the nucleon Fermi gas at low-momentum transfer. This parameter controls the  $Q^2$  distribution in the low  $Q^2$  region only.

In the region of high  $Q^2$  the data excess is observed, and the value of the axial vector mass  $M_A$  obtained from a fit to the measured data, are higher than the results of previous experiments. The formal averaging of  $M_A$  values from several experiments, which are very wide spread from 0.7 to 1.3 GeV, was done in Ref.[57]:  $M_A=1.026\pm 0.021$ . This result is also known as the axial mass world average value. K2K obtained the value of  $1.2\pm 0.12$  from the SciFi detector [12] using the water-aluminum mixture as a target, and also the preliminary result  $1.14\pm 0.11$  from the SciBar detector [56] using a scintillator target. The MiniBooNE experiment (scintillator target) found that the data were better described with an adjustment of two parameters  $M_A=1.23\pm 0.20$  GeV and  $\kappa=1.019\pm 0.011$  [1].

Recently the NOMAD experiment [58] extracted the value of  $M_A=1.05\pm 0.02\pm 0.06$  GeV using a carbon target, which is in agreement with the world average value. This result was obtained from the analysis of a measured  $\nu^{12}C$  total CC QE cross section for neutrino energy above  $\approx 4$  GeV, where the cross section 'plateaus' is reasonably well-known. It should be noted that both approaches, i.e. analysis of the shape of the  $Q^2$  distribution and the direct measurement of the total cross section assume, that the vector form factors are known well from the electron scattering experiments. Actually, at  $Q^2 \geq 3$  (GeV/c)<sup>2</sup> the values of the neutron form factors are much less known than those of the proton [59], and the relative contribution from this region to the total cross section increases with neutrino energy.

To study nuclear effects on the  $Q^2$ -distribution, we calculated with  $M_A=1.032$  GeV the inclusive cross sections  $d\sigma/dQ^2$  for neutrino energies  $\varepsilon_\nu=0.5, 0.7, 1.2$  and  $2.5$  GeV and compared them with those for neutrino scattering on a free nucleon. The results for neutrino and antineutrino scattering on carbon are presented in Figs. 4 and 5, respectively, which show  $d\sigma/dQ^2$  as functions of  $Q^2$ . Here, the results obtained in the RDWIA, are compared with cross sections calculated in the PWIA and RFGM. The cross sections for the exclusive reaction are shown as well. In the region  $Q^2 < 0.2$  (GeV/c)<sup>2</sup> the Fermi gas model results

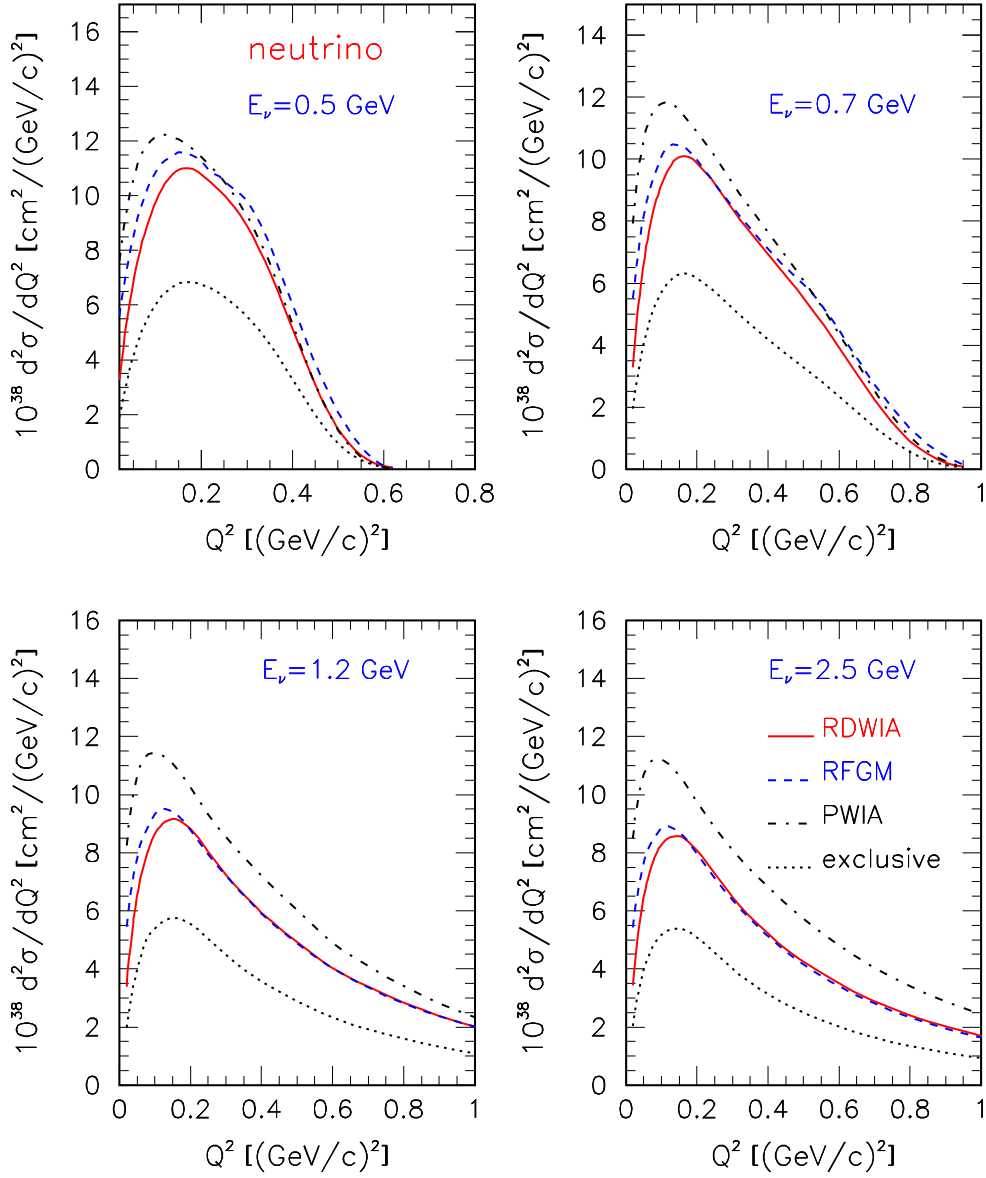


FIG. 4: (Color online) Inclusive cross section vs the four-momentum transfer  $Q^2$  for neutrino scattering off  $^{12}\text{C}$  and for the four values of incoming neutrino energy:  $\varepsilon_\nu=0.5, 0.7, 1.2$ , and  $2.5$  GeV. The solid line is the RDWIA calculation, whereas the dashed and dash-dotted lines are, respectively, the RFGM and PWIA calculations. The dotted lines are the cross sections for the exclusive reaction.

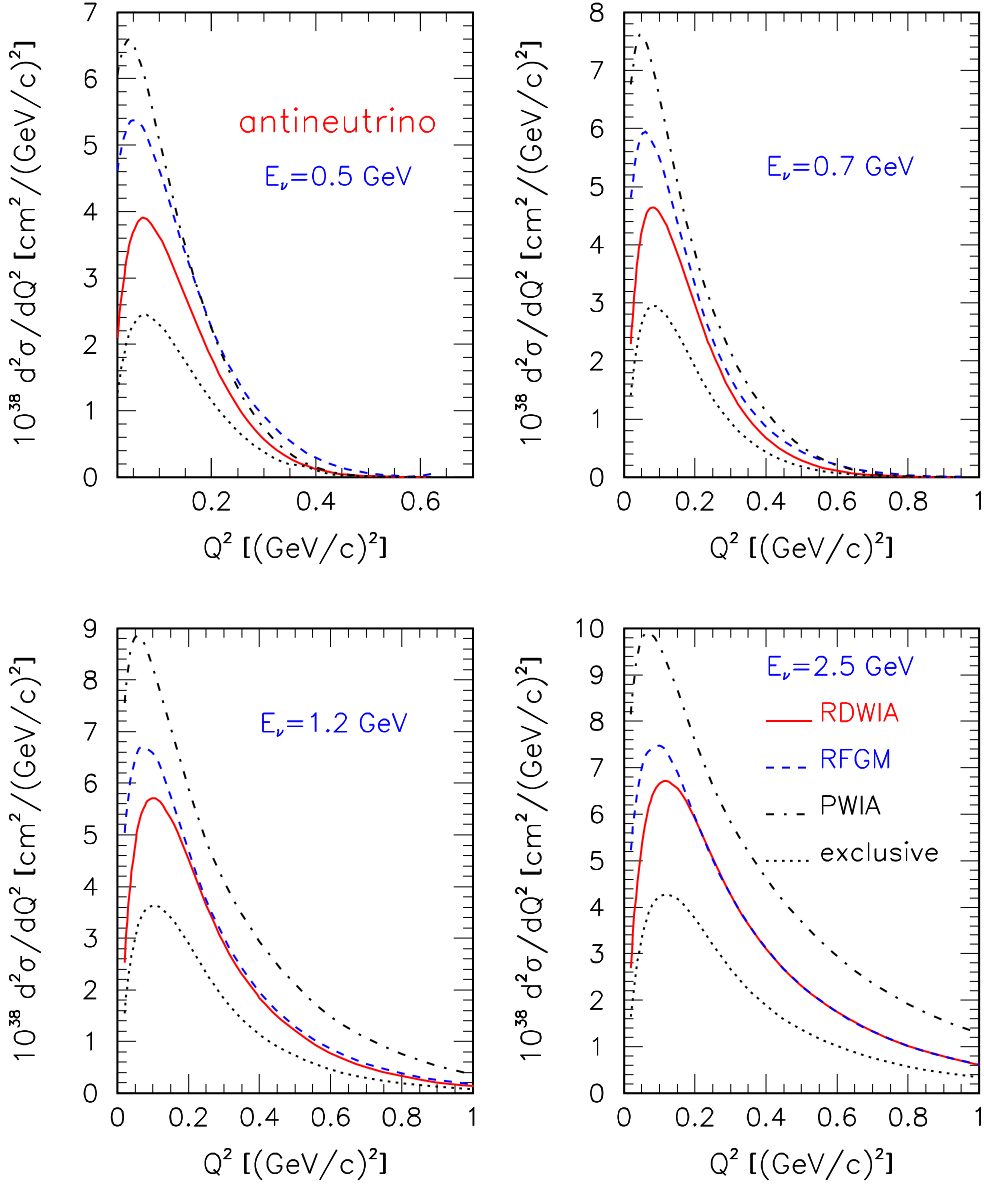


FIG. 5: (Color online) Same as Fig.4, but for antineutrino scattering.

for neutrino (antineutrino) are higher than those obtained within the RDWIA. At  $Q^2=0.1$   $(\text{GeV}/c)^2$  this discrepancy equals 12% (28%) for  $\varepsilon_\nu=0.5$  GeV and decreases to 7% (12%) for  $\varepsilon_\nu=2.5$  GeV. The contribution of  $(\nu, \mu N)$  channels to the inclusive cross sections is about 60%.

Nuclear effects on the shape of the four-momentum transfer  $Q^2$  distribution, i.e. ratio  $R(\varepsilon_\nu, Q^2) = (d\sigma/dQ^2)_{nuc}/(d\sigma/dQ^2)_{free}$ , where  $(d\sigma/dQ^2)_{nuc}$  is the cross section scaled with number of neutron/proton in the target and  $(d\sigma/dQ^2)_{free}$  is the cross section for

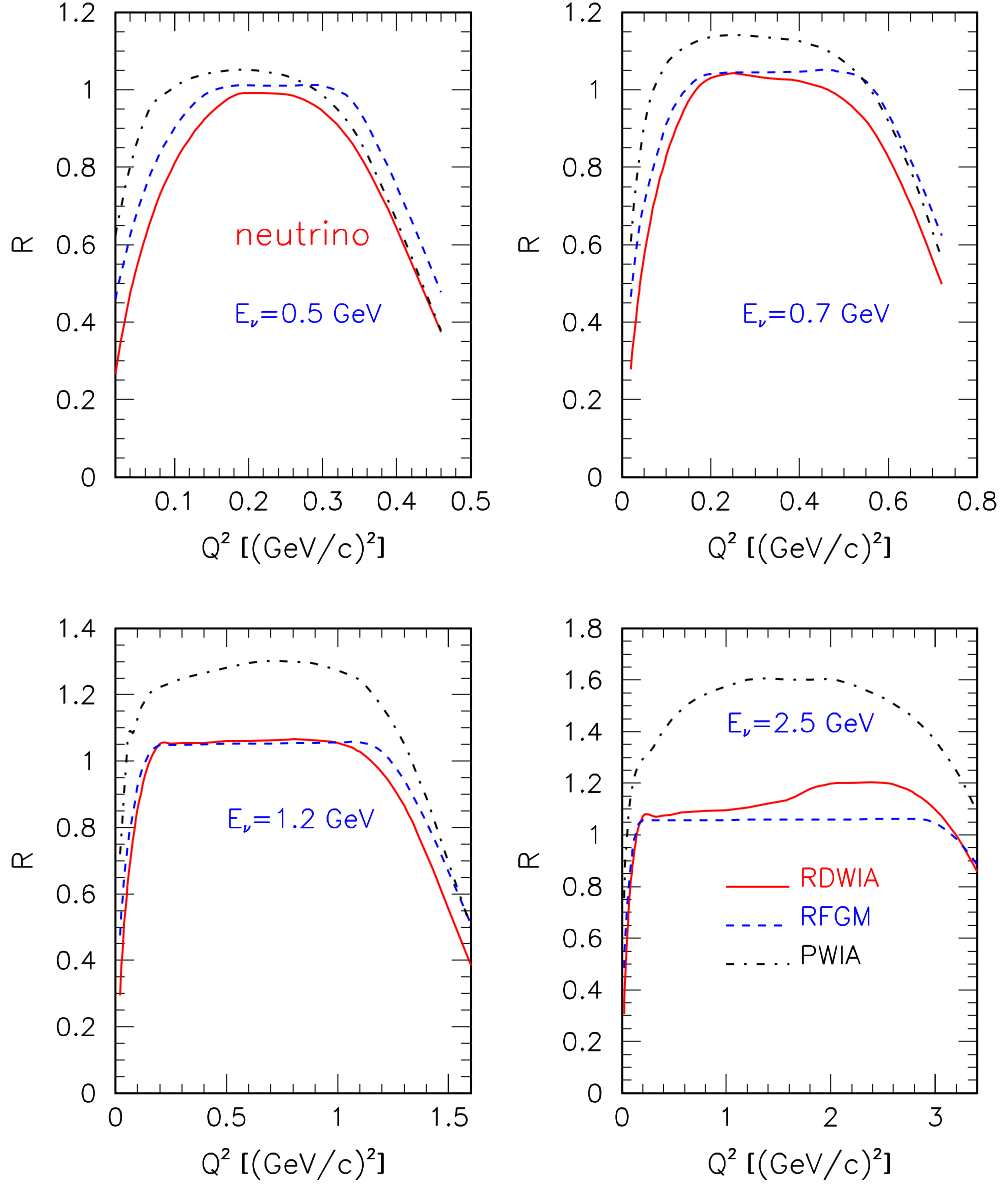


FIG. 6: (Color online) Ratio  $R(\varepsilon_\nu, Q^2)$  vs the four-momentum transfer  $Q^2$  for neutrino scattering off  $^{12}\text{C}$  and for the four values of incoming neutrino energy:  $\varepsilon_\nu=0.5, 0.7, 1.2$ , and  $2.5$  GeV. As shown in the key, the cross sections were calculated with the RDWIA, PWIA, and RFGM.

(anti)neutrino scattering off free nucleon, are presented in Fig. 6 for neutrino and in Fig. 7 for antineutrino as functions of  $Q^2$ . Here, the results obtained in the RDWIA for energies  $\varepsilon_\nu=0.5, 0.7, 1.2$  and  $2.5$  GeV are compared with those calculated in the PWIA and Fermi gas model. The nuclear effects are seen at low  $Q^2$ ; the tail of the momentum distribution at high  $Q^2$ , an overall suppression, and a slight change in the slope in the middle region at



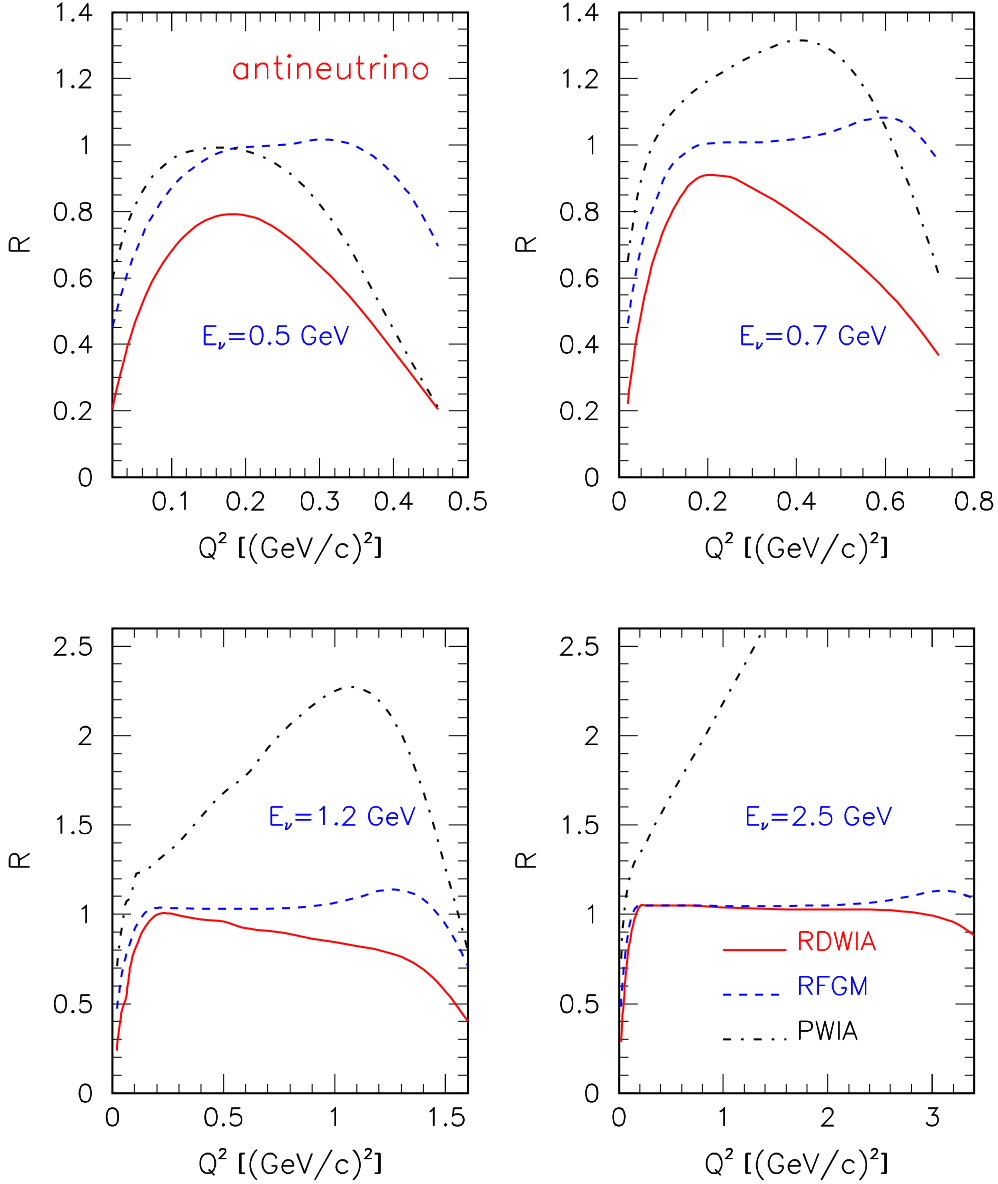


FIG. 7: (Color online) Same as Fig.7, but for antineutrino scattering.

$\varepsilon_\nu \geq 1$  GeV can also be seen. The range of  $Q^2$  where  $R \approx const$ , i.e. nuclear effects are negligible and, therefore cannot modify the value of  $M_A$ , increases with incoming neutrino energy. At energy higher than 1 GeV the range  $0.3 \leq Q^2 \leq 1$  (GeV/c)<sup>2</sup> can be used for  $M_A$  extraction from  $Q^2$  shape-only fit.

We calculated  $d\sigma/dQ^2$  cross sections at energy 700 MeV in the RDWIA and Fermi gas model with  $M_A=1.032$  and 1.32 GeV. The results are shown in Fig. 8 as functions of  $Q^2$ . Apparently at low  $Q^2 \leq 0.1$  (GeV/c)<sup>2</sup> the cross sections depend weakly on the value of the

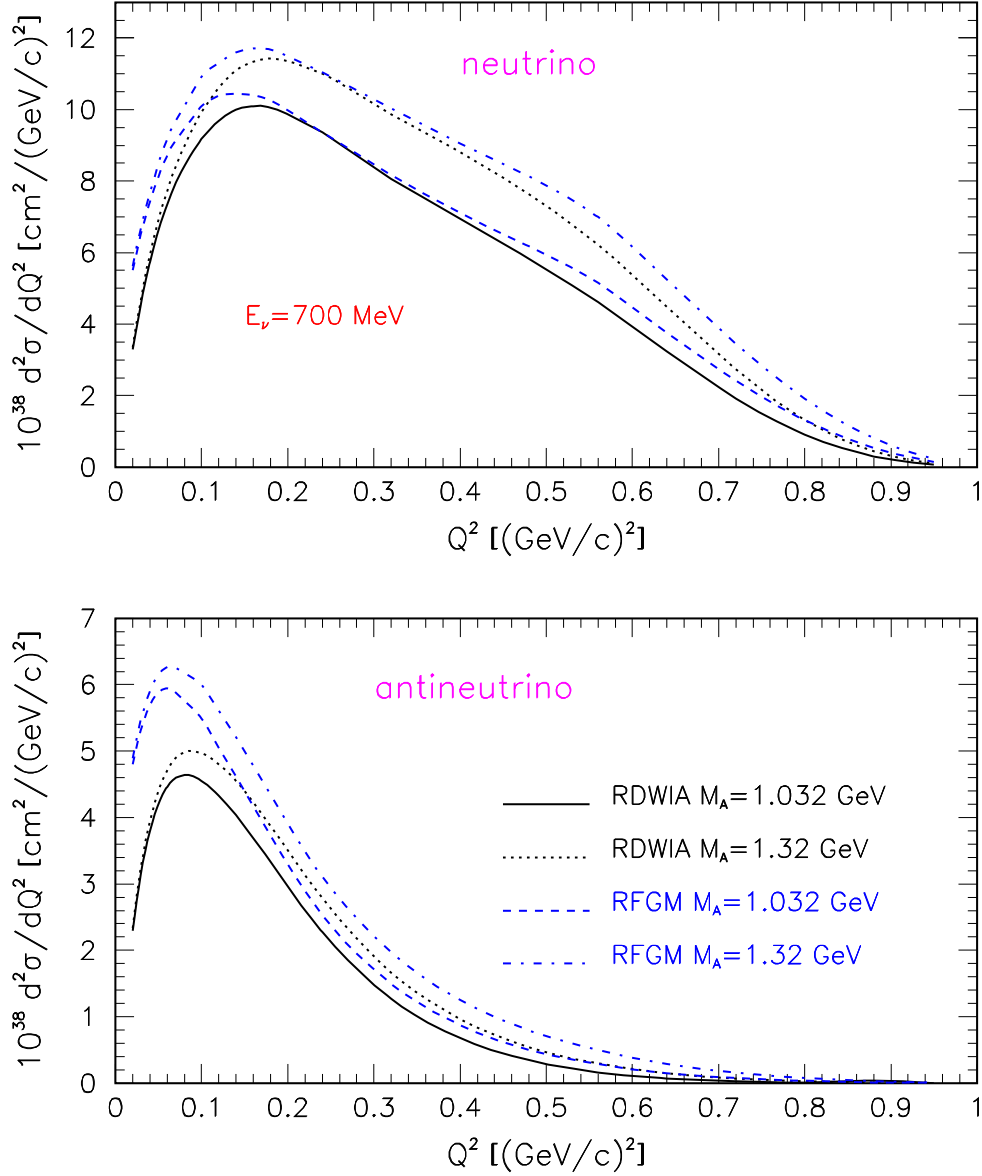


FIG. 8: (Color online) Inclusive cross section vs the four-momentum transfer  $Q^2$  for neutrino (upper panel) and antineutrino (lower panel) scattering off  $^{12}\text{C}$  with energy  $\varepsilon_\nu=0.7$  GeV and for the two values of axial mass  $M_A=1.032$  and  $1.32$  GeV. As shown in the key, cross sections were calculated within the RDWIA and Fermi gas model.

axial mass and  $Q^2$  distributions are controlled by nuclear effects.

The inclusive neutrino and antineutrino cross sections for energies  $\varepsilon_\nu=0.5, 0.7, 1.2,$  and  $2.5$  GeV are presented in Figs. 9 and 10, which show  $d\sigma/d\varepsilon_\mu$  as a function of muon energy. Here, the results obtained in the RDWIA with  $M_A=1.032$  GeV are compared with the

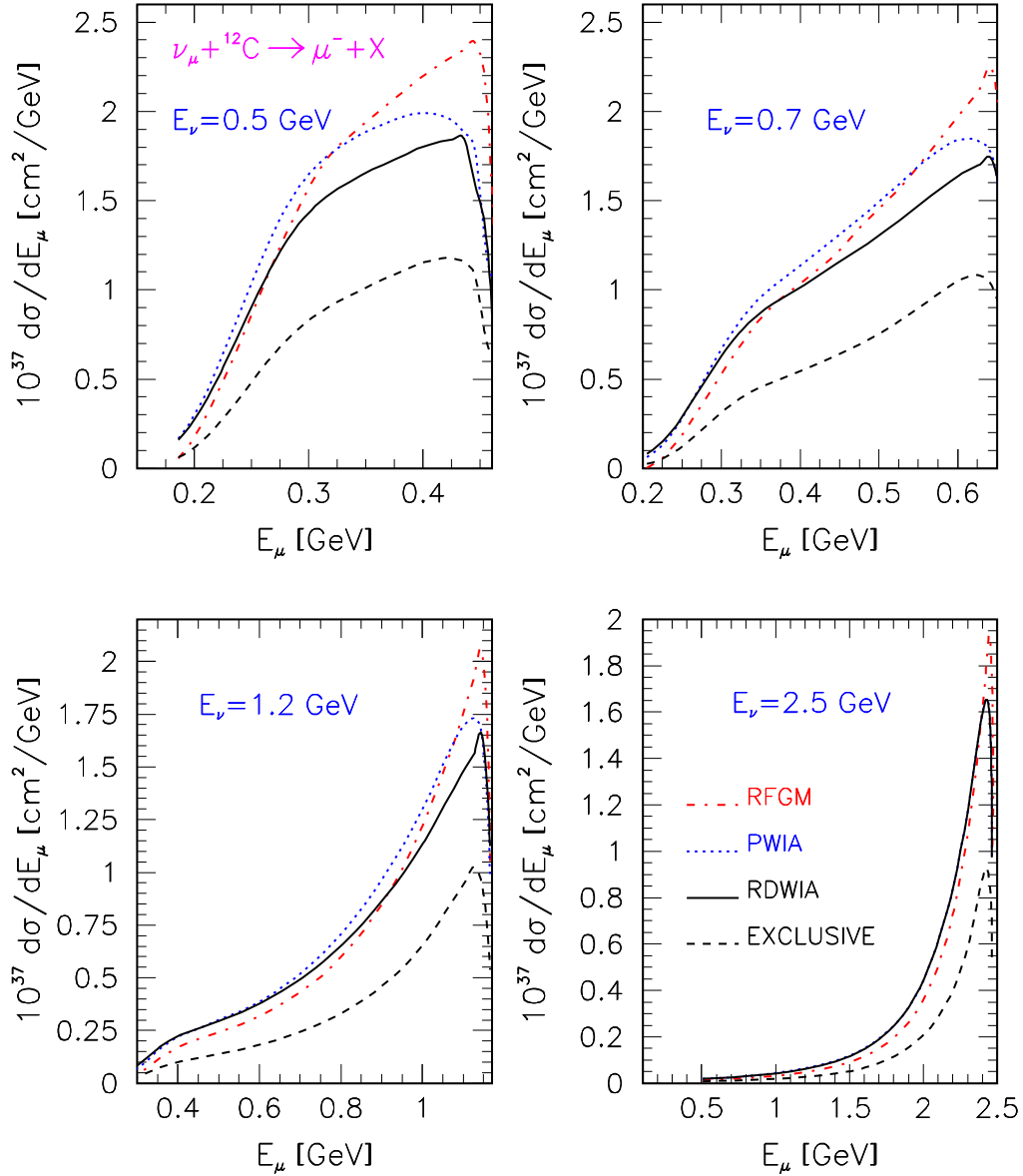


FIG. 9: (Color online) Inclusive cross section vs the muon energy for neutrino scattering on <sup>12</sup>C and for the four values of incoming neutrino energy:  $\varepsilon_\nu=0.5, 0.7, 1.2$ , and  $2.5$  GeV. As shown in the key, the cross sections were calculated with the RDWIA, PWIA, RFGM, and RDWIA for the exclusive reaction.

inclusive cross sections calculated in the PWIA, RFGM, and RDWIA for the exclusive reaction. The cross section values obtained in the RFGM are higher than those obtained within the RDWIA. For neutrino (antineutrino) cross sections in the region close to the maximum this discrepancy is about 25%(49%) for  $\varepsilon_\nu=0.5$  GeV and 23%(29%) for  $\varepsilon_\nu=2.5$

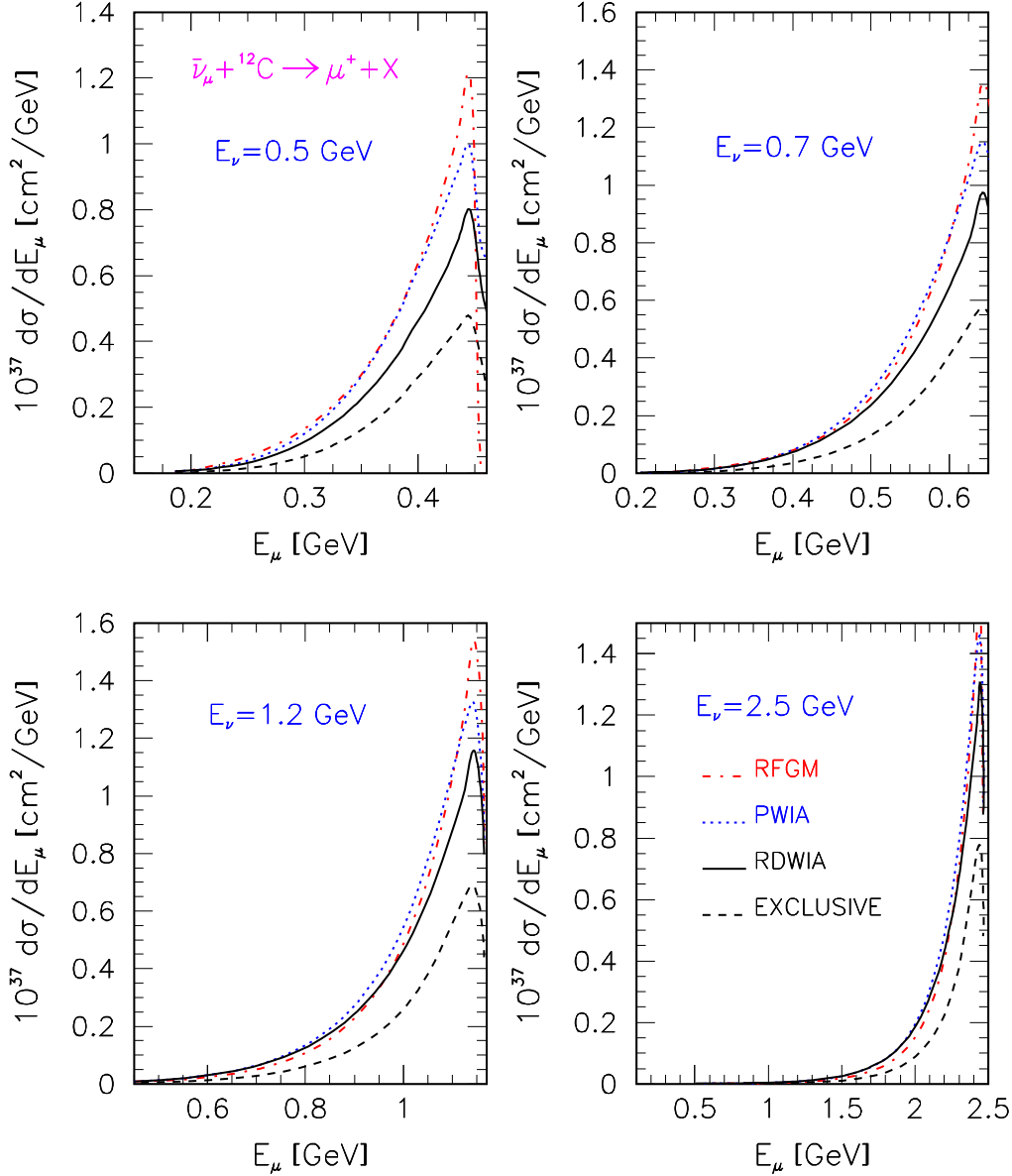


FIG. 10: (Color online) Same as Fig.9, but for antineutrino.

GeV. The contribution of  $(\nu, \mu N)$  channels to the inclusive cross sections is about 60%.

The neutrino and antineutrino total cross sections calculated with  $M_A=1.032$  GeV up to neutrino energy 2.8 GeV, are shown in Fig. 11 together with data of Refs.[60–63]. Also shown are the results obtained in the RFGM, PWIA as well as the contribution of the exclusive channels to the total cross sections. The cross sections are scaled with the number of neutron/proton in the target. The ratio between the neutrino cross sections calculated in the RFGM and RDWIA decreases with neutrino energy from about 1.15 for  $\varepsilon_\nu=0.5$  GeV to

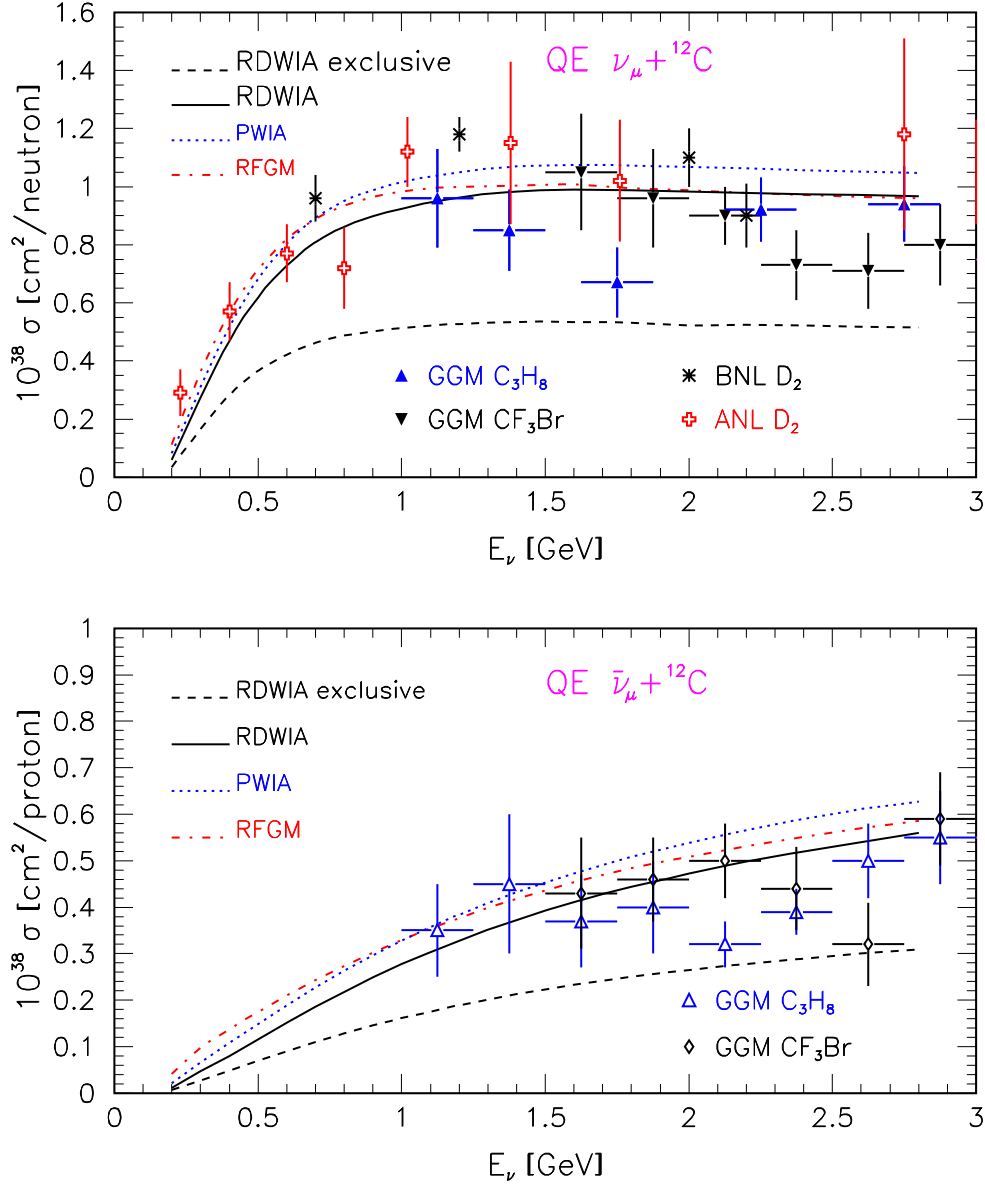


FIG. 11: (Color online) Total cross section for CC QE scattering of muon neutrino (upper panel) and antineutrino (lower panel) on  ${}^{12}\text{C}$  as a function of incoming (anti)neutrino energy. The solid line is the RDWIA result while the dashed-dotted and dotted lines are, respectively, the RFGM and PWIA results. The dashed line is the RDWIA result for exclusive reaction. Data points for different targets are from Refs.[60–63]

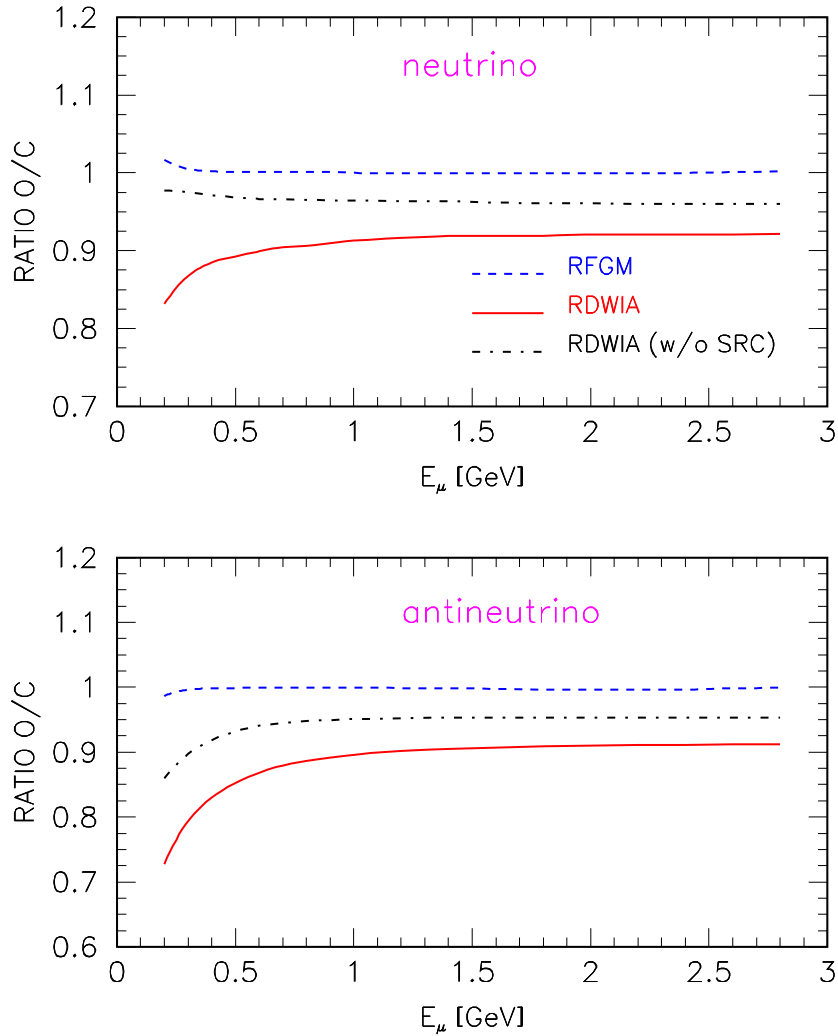


FIG. 12: (Color online) Ratio of the total cross sections per neutron/proton  $R=O/C$  for CC QE scattering of muon neutrino (upper panel) and antineutrino (lower panel) scattering on  $^{16}\text{O}$  and  $^{12}\text{C}$  vs incoming (anti)neutrino energy. The solid line is the RDWIA result, while the dashed and dashed-dotted lines are, respectively, the RFGM and RDWIA without contributions of the short-range correlations.

1.02 for  $\varepsilon_\nu=2.6$  GeV. For the antineutrino cross sections this ratio is about 1.5 for  $\varepsilon_\nu=0.5$  GeV, and 1.05 for  $\varepsilon_\nu=2.6$  GeV. The contribution of the exclusive channels is about 60%. The results presented in Fig.11 show significant nuclear-model dependence for energy less than 1 GeV.

The RDWIA prediction for the CC QE flux-averaged total cross section is compared with

the experimental result from the LSND Collaboration at the Los Alamos for  $^{12}\text{C}(\nu_\mu, \mu^-)$  reaction [64]. The mean energy of the neutrino flux above threshold is 156 MeV. The calculated value of  $10.14 \times 10^{-40} \text{ cm}^2$  well agree with measured value of  $(10.46 \pm 0.3 \pm 1.8) \times 10^{-40} \text{ cm}^2$ .

To compare the CC QE total cross sections for (anti)neutrino scattering on the oxygen [21] and carbon targets, we calculated the ratio  $R(\varepsilon_\nu) = (\sigma_{tot}^O)_{nucl} / (\sigma_{tot}^C)_{nucl}$ , where the cross sections  $(\sigma_{tot}^i)_{nucl}$  are scaled with the number of neutron/proton in the targets. The results obtained in the RFGM and RDWIA are shown in Fig. 12. The Fermi gas model predicts almost identical values of  $(\sigma_{tot}^i)_{nucl}$  for  $^{16}\text{O}$  and  $^{12}\text{C}$ . In the RDWIA approach the cross section calculated for oxygen is lower than that for carbon. For the neutrino (antineutrino) scattering this ratio is 0.90(0.88) at  $\varepsilon_\nu=0.7 \text{ GeV}$  and 0.92(0.91) at  $\varepsilon_\nu=2.6 \text{ GeV}$ .

To study the  $NN$ -correlation effects, we calculated the ratio  $R(\varepsilon_\nu)$  without the  $NN$ -correlation contribution, i.e. with  $S_\alpha=1$  for all bound nucleon states in the oxygen and carbon targets. The difference between results obtained with and without the high-momentum component contribution is about 5% for  $\varepsilon_\nu \geq 1 \text{ GeV}$ . In Ref.[21] was shown that the  $NN$ -correlation effect reduces the total cross section in proportion to the missing strength in the nuclear ground state, which is about 25% for  $^{16}\text{O}$  and 11% for  $^{12}\text{C}$ .

Therefore in the long-base line neutrino oscillation experiments a part of the near detector must include some of the same target material, as the far detector to reduce the systematic uncertainty due to nuclear effects on the CC QE total cross section.

#### IV. CONCLUSIONS

In this paper, we study electron and CC quasi-elastic (anti)neutrino scattering on a carbon target in different approximations (PWIA, RDWIA, RFGM) placing particular emphasis on the nuclear-model dependence of the results. In RDWIA, the LEA program, adapted to neutrino interactions, was used to calculate the differential and reduced exclusive cross sections. We found that the reduced cross sections for (anti)neutrino scattering are similar to those of electron scattering and the latter are in a good agreement with electron data. In calculating the inclusive and total cross sections, the imaginary part of a relativistic optical potential was neglected and the SRC effect in the target ground state was taken into account. This approach was tested against electron-carbon inclusive scattering data. This test revealed an overall agreement with the data, with the differences between calculated

and measured cross sections in the peak region less than 12%.

We calculated  $d\sigma/dQ^2$  cross sections for different neutrino energies and estimated the range of  $Q^2$  where nuclear effects on the shape of  $Q^2$  distribution are negligible. Also was shown that at low  $Q^2 < 0.1 \text{ (GeV/c)}^2$  the cross sections depend weakly of the values of the axial mass.

The CC QE total cross sections predicted by the RFGM are higher than the corresponding values obtained in the RDWIA and this difference decreases with neutrino energy. The flux-averaged total cross section was calculated within the RDWIA approach and compared with the experimental result from the LSND Collaboration. The calculated cross section is in good agreement with data. We compared the CC QE total cross sections (scaled with the number of neutron/proton in the target) for (anti)neutrino scattering on the oxygen and carbon targets and found that the cross sections calculated within the RDWIA for oxygen, are lower than those calculated for carbon, and the SRC effects increase this difference.

We conclude that the data favor the RDWIA results. This indicates that the use of RDWIA in Monte Carlo simulations of the neutrino detector response would allow one to reduce the systematic uncertainty in neutrino oscillation parameters.

### Acknowledgments

The author greatly acknowledges S. Kulagin, J. Morfin, G. Zeller, N. Jachowicz, M. Wascko, R. Gran, and T.Katori for fruitful discussions at different stages of this work.

- 
- [1] A. A. Aguilar-Arevalo *et al.*, (MiniBooNE Collaboration), Phys. Rev. Lett. **100**, 032301 (2008).
  - [2] AK.Hiraide *et al.*, (SciBooNE Collaboration), Phys.Rev. **D78**, 112004 (2008).
  - [3] P. Adamson *et al.*, (MINOS Collaboration), Phys. Rev.**D77**, 072002 (2008).
  - [4] K. S. McFarland *et al.*, (MiNERvA Collaboration), Nucl. Phys. B (Proc. Suppl.) **159**, 107 (2006).
  - [5] T. Nakadaira *et al.*, (T2K Collaboration), Nucl. Phys. B (Proc. Suppl.) **149**, 303 (2006).
  - [6] G. Rosa *et al.*, (OPERA Collaboration), Nucl. Phys. B (Proc. Suppl.) **145**, 98 (2005).



- [7] D. S. Ayres *et al.*, (NOvA Collaboration), arXiv:hep-ex/0503053.
- [8] A. Vacheret *et al.*, (T2K Collaboration), AIP (Conf. Proc.) **967**, 66 (2007).
- [9] G. P. Zeller, arXiv:hep-ex/0312061.
- [10] R. A. Smith and E. J. Moniz, Nucl. Phys. **B43**, 605 (1972); *erratum: ibid.* **B101**, 547 (1975).
- [11] A. V. Butkevich and S. P. Mikheyev, Phys. Rev. **C72**, 025501 (2005).
- [12] R. Gran *et al.*, (K2K Collaboration), Phys. Rev. **D74**, 052002 (2006).
- [13] O. Benhar, N. Farina, H. Nakamura, M. Sakuda, and R. Seki, Phys. Rev. **D72**, 053005 (2005).
- [14] O. Benhar and D. Meloni, Nucl. Phys. **A789**, 379 (2004).
- [15] A. Meucci, C. Giusti, and F. D. Pacati, Nucl. Phys. **A739**, 277 (2004).
- [16] A. Meucci, C. Giusti, and F. D. Pacati, Nucl. Phys. **A744**, 307 (2004).
- [17] A. Meucci, C. Giusti, and F. D. Pacati, Phys. Rev. **C77**, 034606 (2008).
- [18] C. Maieron, M. C. Martinez, J. A. Caballero, and J. M. Udias, Phys. Rev. **C68**, 048501 (2003).
- [19] M. C. Martinez, P. Lava, N. Jachowicz, J. Ryckebusch, K. Vantournhout, and J. M. Udias, Phys. Rev. **C73**, 024607 (2006).
- [20] N. Jachowicz, P. Vancraeyveld, P. Lava, C. Praet, and J. Ryckebusch, Phys. Rev. **C76**, 055501 (2007).
- [21] A. V. Butkevich and S. A. Kulagin, Phys. Rev. **C76**, 045502, (2007).
- [22] A. V. Butkevich, Phys. Rev. **C78**, 015501 (2008).
- [23] K. S. Kim, B. G. Yu, M. K. Cheoun, T. K. Choi, and M. T. Chung, J. Phys. **G34**, 2643 (2007).
- [24] K. S. Kim, M. K. Cheoun, and B. G. Yu, Phys. Rev. **C77**, 054604 (2008).
- [25] J. Nieves, J. E. Amaro, and M. Valverde, Phys. Rev. **C70**, 055503 (2004).
- [26] J. Nieves, M. Valverde, and M. J. Vicente Vacas, Phys. Rev. **C73**, 025504 (2006).
- [27] M. S. Athar, S. Chauhan, S. K. Singh, and M. J. Vicente Vacas, arXiv:0808.1437 [nucl-th].
- [28] M. S. Athar, S. Chauhan, and S. K. Singh, arXiv:0808.2103 [nucl-th].
- [29] J. E. Amaro, M. B. Barbaro, J. A. Caballero, and T. W. Donnelly, Phys. Rev. Lett. **98**, 242501 (2007).
- [30] J. E. Amaro, M. B. Barbaro, J. A. Caballero, T. W. Donnelly, and J. M. Udias, Phys. Rev. **C75**, 034613 (2007).
- [31] M. C. Martinez, J. A. Caballero, T. W. Donnelly, and J. M. Udias, Phys. Rev. **C77**, 064604 (2008).

- [32] T. Leitner, O. Buss, L. Alvarez-Ruso, and U. Mozel, arXiv:0812.0587 [nucl-th].
- [33] J. J Kelly, <http://www.physics.umd.edu/enp/jjkelly/LEA>
- [34] C. Ciofi degli Atti and S. Simula, Phys. Rev. **C53** , 1689, 1996.
- [35] S. A. Kulagin and R. Petti, Nucl. Phys. **A765**, 126, 2006.
- [36] T. de Forest, Nucl. Phys. **A392**, 232, 1983.
- [37] P. Mergell, U.-G. Meissner, and D. Drechsel, Nucl. Phys. **A596**, 367, 1996.
- [38] J. J. Kelly Phys. Rev. **C59**, 3256 (1999).
- [39] B. Serot, J. Walecka, Adv. Nucl. Phys. **16**, 1, 1986.
- [40] C. J. Horowitz D. P. Murdock, and Brian D. Serot, in *Computational Nuclear Physics 1: Nuclear Structure* edited by K. Langanke, J. A. Maruhn, Steven E. Koonin (Springer-Verlag,Berlin, 1991), p.129
- [41] J. J. Kelly Phys. Rev. **C71**, 064610 (2005).
- [42] D. Rohe *et al.*, Nucl. Phys. B (Proc. Suppl.) **159**, 152 (2006).
- [43] T. Frick, K. Hassaneen, D. Rohe, and H. Müther, Phys. Rev. **C70**, 24309 (2004).
- [44] O. Benhar, A. Fabrocini, and S. Fantoni, Phys. Rev. **C41**, R24 (1990).
- [45] J. M. Udias, P. Sarriguren, E. Moya de Guerra, E. Garrido, and J. A. Caballero, Phys. Rev. **C51**, 3246 (1995).
- [46] M. Hedayati-Poor, J. I. Johansson, and H. S. Sherif, Phys. Rev. **C51**, 2044 (1995).
- [47] E .D. Cooper, S. Hama, B. C. Clark, and R. L. Mercer, Phys. Rev. **C47**, 297 (1993).
- [48] S. Frullani and J. Mougey, Adv. Nucl. Phys. **14**, 1 (1984).
- [49] D. Dutta *et al.*, Phys. Rev. **C68**, 064603, (2003).
- [50] A. Meucci, F.Capuzzi, C. Giusti, and F. D. Pacati, Phys. Rev. **C67**, 054601 (2003).
- [51] D. Baran *et al.*, Phys. Rev. Lett. **61**, 400, (1988).
- [52] J. S. O’Connel *et al.*, Phys. Rev. **C35**, 1063, (1987).
- [53] R. R. Whitney, I. Sick, J. R. Ficenecc, R. D. Kephart, and W. P. Trower, Phys. Rev. **C9**, 2230, (1974).
- [54] P. Barreau *et al.*, Nucl. Phys. **A402**, 515, (1983).
- [55] D. Day *et al.*, Phys. Rev. **C48**, 1849, (1993).
- [56] X. Espinal, F. Sanchez, AIP (Conf. Proc.) **967**, 117 (2007).
- [57] V. Bernard, L. Elouadrhiri, U. G. Meissner, J. Phys. **G28**, R1, (2002).
- [58] V. Lyubushkin *et al.*, (NOMAD Collaboration), arXiv:0812.4543 [hep-ex].

- [59] H. Budd, A. Bodek, J. Arrington, arXiv:hep-ex/0308006.
- [60] W. A. Mann *et al.*, Phys. Rev. Lett. **31**, 844, (1973).
- [61] N. J. Baker *et al.*, Phys. Rev. **D23**, 2499, (1981).
- [62] M. Pohl *et al.*, Lett. Nuovo Cim. **26**, 332, 1979.
- [63] J. Brunner *et al.*, Z. Phys. **C45**, 551, 1990.
- [64] L. B. Auerbach *et al.*, Phys. Rev. **C66**, 015501, (2002).